Article

Not peer-reviewed version

Design of a Solar Dish Receiver and Life Cycle Assessment of a Hot Water Production System

Ibrahim Tursunović and Davide Papurello *

Posted Date: 17 November 2023

doi: 10.20944/preprints202311.1161.v1

Keywords: Concentrated Solar Power; Domestic hot water; Life Cycle Assessment; Renewable energy

Article

Design of a Receiver for Solar Parabolic Dish and Life Cycle Assessment of Domestic Hot Water Production System

Ibrahim Tursunović [1] and Davide Papurello [1,2,*]

[1] Department of Energy (DENERG), Politecnico di Torino, Corso Duca degli Abruzzi, 24, 10129, Turin, Italy
[2] Energy Center, Politecnico di Torino, Via Paolo Borsellino 38/16, 10138 Turin, Italy
* Correspondence: davide.papurello@polito.it

Abstract: Since the energy sector is the main source of greenhouse gases, it has the highest potential for improvement. Improvements can be achieved by generating energy from renewable sources. Combined with thermal energy storage, concentrating solar power plants represent a promising technology for dispatchable renewable energy, ensuring a stable energy supply even in remote areas without contributing to greenhouse gas emissions during operation. However, it is important to note that greenhouse gases and other polluting emissions may occur during the manufacturing process of concentrating solar power plant components. This work analyses the design of the receiver to produce thermal energy for the existing solar dish CSP plant at the Energy Center of the Politecnico di Torino. The objective of this plant is to produce hot water for a small case study. Considering the average solar irradiance for Turin equal to 800 W/m2, the surface heat flux was obtained from the first part of the analysis, which was used to obtain the maximum internal temperature in the receiver equal to 873.7 °C. The maximum temperature obtained was a constraint for the selection of the material for the solar receiver. Of the various possibilities, copper was chosen. In the second part of the work, a Life Cycle Assessment was carried out to compare the emissions generated during the production of the main components of the CSP plant with the emissions generated by the methane-fuelled water heater that produces the same amount of water as the CSP plant. It can be concluded that the manufacture of the main components of the CSP plant results in lower greenhouse gas emissions than the operational phase of a conventional natural gas-fired water heater (1.6 kg CO2/day).

Keywords: concentrated solar power; domestic hot water; life cycle assessment; renewable energy

Introduction

The European Green Deal seeks to make Europe the first carbon-neutral continent by 2050 and reduce GHG emissions by at least 55% by 2030 [1]. These goals are achievable through a broad energy transition in different sectors. Five emission sectors have been identified, and in Europe, the main one is the transport sector (28%) [2]. The energy transition, which is widely studied and debated, will bring many benefits, such as increased energy reliability, economic growth, and job creation [3,4]. Gielen et al., pointed out that the use of renewable energies, and improved conversion factor, together with electrification of end uses, account for 94% of emission reductions [3]. Although energy use for heating has remained stable since 2010, production systems are mostly powered by fossil fuels. The share powered by renewable energy is around 20% in 2019 [5]. To meet Sustainable Development Scenario (SDS) objectives, clean energy technologies must exceed 50% of new heating equipment sales by 2030 [6]. Heating and hot water account for 79% of total final energy use in EU countries [7]. Solar energy, especially Concentrated Solar Power (CSP), can play a crucial role in this context, particularly for district heating networks in local communities [8–10]. Solar energy is used in Solar District Heating (SDH) projects across Europe, contributing up to 20% of annual heat demand, and potentially more with seasonal storage [11]. Among CSP technologies, the dish system offers high thermal efficiency for medium to high temperatures and is suitable for high-temperature applications [12]. Efficient energy conversion is achieved with sun-tracking parabolic dish collectors and cavity

 doi:10.20944/preprints202311.1161.v1

receivers, minimizing heat losses [13]. Parabolic dish collectors exhibit superior energy conversion efficiency among CSP systems, as investigated by Coventry et al., [14]. However, each dish has a relatively low thermal power output, often in the tens of kilowatts. A positive aspect is the possibility of producing thermal and electrical energy in a combined way. These characteristics make dishes particularly attractive for domestic applications, small buildings and local communities. However, dish technology is not widely adopted, there is a need to extend the stability of conversion efficiency to increase commercial penetration [15]. Only a few studies focus on the heating part of CSPs [14]. Coventry et al., highlighted the operation of an ARUN system (2016), where an output of the system in addition to electricity is also the production of pressurised hot water, which can be used in a thermal energy distribution network [14].

This work primarily involves evaluating the performance of an existing CSP dish located at the Energy Center of Politecnico di Torino. One of the main objectives of this study is to also study thermal energy production with the CSP, after previous publications related to the electricity production [16–19]. The CSP dish is integrated with a water storage tank, forming a system designed to provide hot water for integration into the Energy Centre's network. In the second part of the paper, a comprehensive life cycle analysis (LCA) will be conducted on the key components of the entire system used. In particular, the proposed configuration does not incorporate any fossil-based backup heating sources, ensuring no pollutant emissions during system operation. Therefore, the LCA presented here will focus on the entire life cycle of the main components, from their initial production to their eventual disposal. The main components considered in the analysis include the solar collector, the solar receiver, the domestic hot water tank, and the piping system.

Material and methods

The concentrator consists of a single solar dish with an aperture of approximately 2.4 m (Elma net. Srl, TN). The system is composed of two motors to allow optimal orientation according to the time of day, and from the geographical coordinates of the site where the CSP is installed (Turin, 45.0676 N, 7.6563 E). Other useful geometric and technical parameters are listed in the following table (Table 1), and in previous studies [18,20].

Table 1. Features of the solar dish concentrator.

	Description	Value	Unit of measure
D_c	Diameter of the dish	2370	mm
f	Focal distance	958	mm
y_R	Depth	370	mm
$\boldsymbol{\varphi_R}$	Rim angle	61.89	°
Co	Optical Concentration ratio	8013	-
d_f	Diameter of the focal point	6.41	mm
l	Length of the receiver	200	mm
A	Area of the concentrator	4.5	m^2
P	Power of the concentrator	2.8	kW

The concentrator-receiver system is built using Comsol multiphysics Inc. software (Sweden). In this work, an average value was set for the global irradiance (800 W/m²). This value is derived from previous experimental measurements conducted in the plant and recently published [16]. If the dish were a perfect reflector, i.e., if all incoming radiation were reflected specularly, if the dish were perfectly smooth and if the sun's rays behaved as planar waveforms from an infinitely distant point source, all incoming rays would focus on a single point in the collector - in the focus of the paraboloid. To make the system more realistic, some deviations from the ideal case were included in the analysed model:

- Part of the incoming radiation is absorbed by the dish. In this model, the absorption coefficient is set to 0.1, which means that 90% of the incoming radiation is reflected.

 doi:10.20944/preprints202311.1161.v1

- Not all incident rays will be parallel; instead, the incident rays are sampled by a narrow cone with a maximum angle, ψm, of 4.56 mrad. In practice, a part of the radiation is also emitted from the circumsolar region surrounding the solar disc, instead of from the solar disc itself, but this radiation is neglected in the present model, i.e. a circumsolar ratio (CSR) of zero is assumed.
- Since the surface of the parabola is not perfectly smooth, the reflected rays are not all released in the same direction. Instead, the surface normal is perturbed by an additional angle that is sampled by a Rayleigh distribution. This optical error is taken into account with a surface tilt error of 1.75 mrad.
- The limb darkening effect is considered to consider the variation in power of rays from different regions of the Sun. In particular, the rays emitted from the centre are more intense than those emitted from the peripheral regions of the solar disc.
- Rays are released from 250000 distinct points.

In the present work, a cavity solar receiver was chosen for its simplicity and ease of fabrication, see Figure 1 and Figure 2. The mesh must have a higher resolution on curved surfaces to accurately represent the surface normal. On the other hand, the mesh on flat surfaces can be coarser. A fine mesh on curved surfaces improves the accuracy of the reinitialised wave vectors of reflected and refracted rays [21]. To reduce the mesh size on the curved surfaces without creating superfluous meshes, a curvature factor of 0.2 was selected. Furthermore, since the main objective is to determine the temperature distribution within the receiver, a customised free triangular mesh was used on the receiver with a maximum element size of $2E^{-4}$ [mm] and a minimum element size of $4E^{-5}$ [mm].

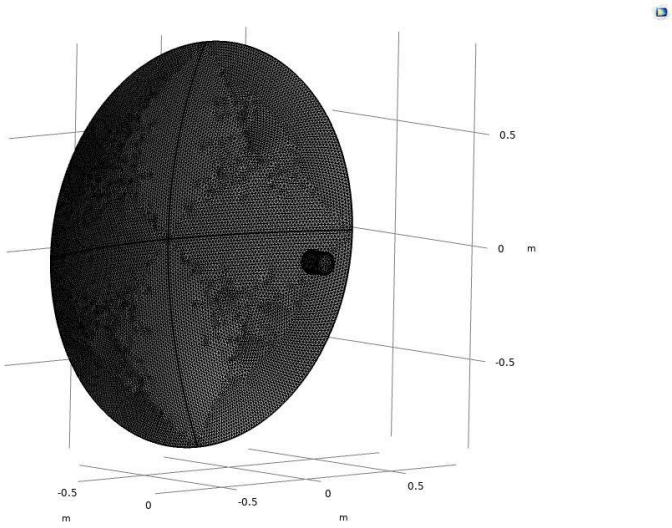

Figure 1. Mesh representation of the CSP with the cavity receiver in COMSOL.

The shape and dimensions of the receiver, the solar absorptance of its inner surface, and the type of reflection on its inner surface, in conjunction with the parameters introduced earlier, collectively influence the uneven absorption of heat flux by the receiver's inner surface. These factors play a crucial role in determining the actual distribution of absorbed radiant flux density.

Preprints (www.preprints.org) | NOT PEER-REVIEWED | Posted: 17 November 2023 doi:10.20944/preprints202311.1161.v1

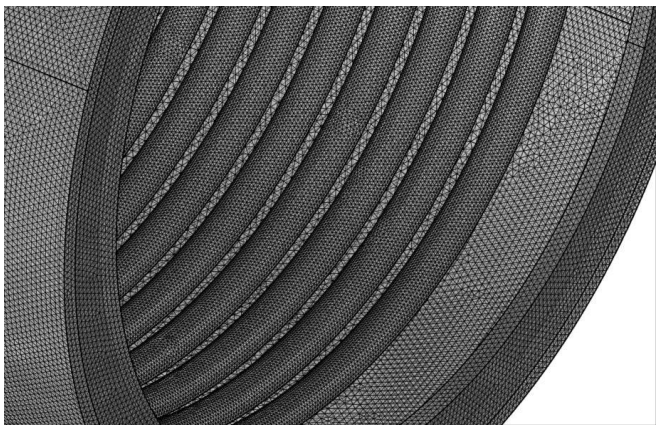

Figure 2. Mesh representation of the receiver's inner surface.

The mesh independence analysis was accomplished using the same procedure reported in Marra et al., [16]. The model built was validated with experimental temperature measured inside the receiver structure using a B-type thermocouple (Tersid srl, Italy). The system modelled (CSP + cavity receiver) is connected to a water storage tank to meet the hot water needs. Thermal demand for domestic hot water can be expressed by the following equation:

$$Q_{DHW} = \dot{m} \cdot c_p \cdot (T_{use} - T_{mains}) \qquad \text{(eq. 1)}$$

Where $\dot{m}$, is the daily demand of DHW in $\frac{kg}{s\ person}$; temperature, T_{use} can be generally assumed to be in the range $40 \div 50\,°C$. While the temperature from the aqueduct is related to the average temperature of the ground at $1 \div 2\,m$ depth. In Italy T_{mains} vary between $12 \div 14\,°C$ in the Po Valley. The demand for DHW is equal to around $27000\ \frac{kJ}{day}$ or $7.5\ \frac{kWh}{day}$ for the selected case study. An important aspect related to the performance of a TES is maintaining a high degree of stratification of the reactor volume connected to the users. Thermal stratification allows a limited operation of the auxiliary energy supply. For sensible TES the lower and upper temperature limits determine the maximum storage capacity. However, maximum storage capacities are not accessible in real storage systems [22].

Dimensioning of storage is based on the following equation:

$$V = \frac{Q}{\rho \cdot c_p \cdot (T_{max} - T_{min})} \qquad \text{(eq. 2)}$$

Where Q is the thermal energy demand, T_{max} is the maximum temperature in the tank ($80 \div 85\,°C$ for non – pressurized water tank), T_{min} is the minimum temperature for satisfying the demand ($45 \div 55\,°C$) [22]. In this work, maximum tank temperature was set to $80\,°C$ (to prevent legionella disease) and minimum to $45\,°C$ and using DHW demand previously calculated, a volume of $190\,l$ is sufficient.

Energy demand for heating this volume of water can be evaluated by the following equation:

$$E = m \cdot c_p \cdot \Delta T \qquad \text{(eq. 3)}$$

Where E is the amount of thermal energy demanded to heat water, m is the water tank dimension, c_p is the specific heat of the water, while ΔT is equal to 15 °C.

$$E = 190 \cdot 1{,}16 \cdot 10^{-3} \cdot 35 = 7.71\ kWh \qquad \text{(eq. 4)}$$

In the second part of the paper, a life cycle analysis was performed. Despite the widespread use of concentrating solar power plants, their environmental assessment is still little investigated. Reviewing the literature studies on the LCA of CSP, it can be seen that most of the references concern CSP plants based on parabolic troughs and solar tower technology [23–25]. Leamnatou et al. state that the impact of CSP plants depends on the use of water and the materials used for storage.

Preprints (www.preprints.org) | NOT PEER-REVIEWED | Posted: 17 November 2023 doi:10.20944/preprints202311.1161.v1

Carnevale et al. presented a general case of LCA of solar energy systems [26,27]. By reviewing the literature, further investigations are needed on plate systems, storage materials, water-saving strategies, and the soiling effect, for even small systems focused on small CSP systems.

This analysis aims to study the impacts of a solar parabolic dish (CSP) used for energy production from cradle to grave, as in literature there are not any similar studies. LCA analysis is done on macro components of the system. These components are solar parabolic dish, solar receiver, water storage tank and pipes. This choice is due to several limitations, one of which is the database used. As the database has limited sources, electronic components were excluded from the analysis - the same applies to the welding of parts. The functional unit chosen in this study is "a hot water tank" and, in accordance with ISO 14040 and 14044, the results of the LCA are expressed in terms of this functional unit.

The system boundary shown in Figure 3 includes the production, utilisation, and final decommissioning phases. Four different processes were considered separately to produce the system. Each of the processes includes raw material extraction and end-of-life treatment. The process "Parabola for hot water production" represents a process that includes all the outputs of the previous processes. In fact, it includes four upstream processes as inputs and their transport from the production site to the utilisation site. The output of the process "Parabola for domestic hot water production" is the input of "Domestic hot water production", together with "water". The last process is the functional unit to which all results will be referred: a domestic hot water tank. In this last process, which represents the utilisation phase, water consumption is also included. In this case, the transport of water from the extraction source to the point of use is not considered. The manufacturing processes of the hot water tank, receiver, piping and solar collector do not include the impacts of their assembly. These impacts were omitted due to a lack of reliable data. Furthermore, due to the difficulty of finding accurate information on the quantities of materials used, the analysis was based on product data sheets and estimates from the literature. The life expectancy of the components is assumed to be 30 years. Assuming that a tank full of water is consumed every day, the consumption can be translated into 10950 days. If the tank operates for 255 days per year and considering, the previously introduced functional unit - a domestic hot water tank - the weight of one day of operation is equal to 1.307E-4 of the life expectancy, see Figure 4. Since the dish under analysis is in Turin, Italy, whenever possible, the processes used for data representation were in Italy, Europe or a European country. The software used is openLCA 1.10.3 (GreenDelta GmbH, Germany) and the database is version 1.00 of the open-source Environmental Footprint database.

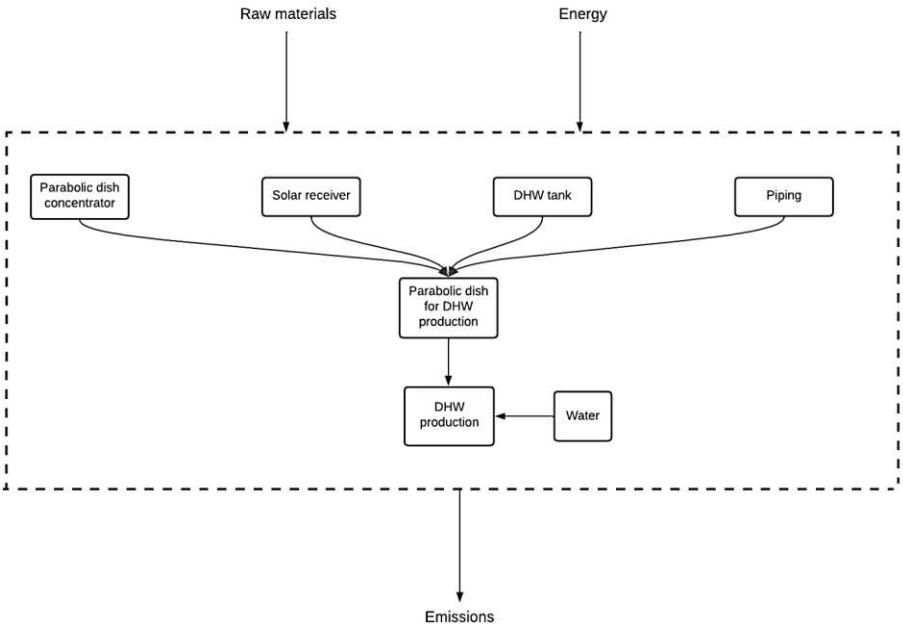

Figure 3. LCA Boundary system representation.

Preprints (www.preprints.org) | NOT PEER-REVIEWED | Posted: 17 November 2023 doi:10.20944/preprints202311.1161.v1

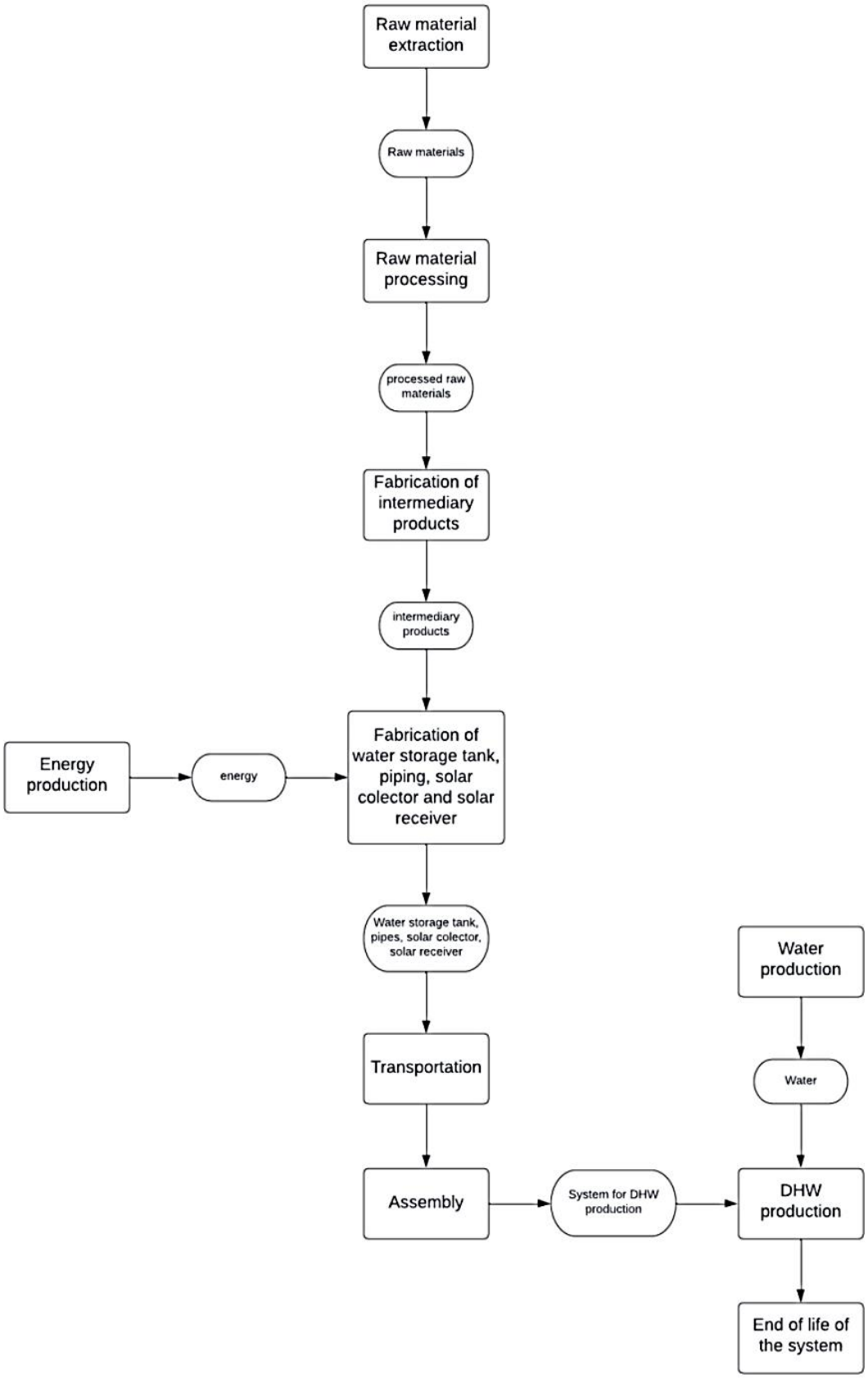

Figure 4. Flowchart of the system.

 doi:10.20944/preprints202311.1161.v1

Results and discussion

Material selection and quantification for LCA

The tanks used to contain the water are made of steel with cathodic corrosion protection of the galvanic type. This is necessary to consider the thermal variation during the operation of the system. Magnesium anodes were chosen. Geometrical data and material specifications for the other components were taken from data sheets and materials readily available in the database, see Table 2.

Table 2. Hot water tank materials.

Material	Unit	Value	
Stainless steel	kg	104.75	Value estimated from technical sheet
Aluminium	kg	4.4	Value estimated considering aluminium density, heat exchanger surface and thickness
Magnesium	kg	0.5	Value found in literature [28,29]
Rigid expanded polyurethane	kg	8.3	Value estimated considering data from technical specifications of water storage tank [30,31]
PVC	kg	1	Estimated weight of plastics
Alkyd paint	kg	1.05	Value estimated considering the water storage geometry, paint density and thickness [32,33]

The Life Cycle Assessment (LCA) considers also pipes, for conveying water from the receiver to the tank. The assumption here is that the hot water storage tank is positioned at 2 meters from the receiver, and these pipes are constructed using polypropylene reinforced with fibreglass. External thermal insulation is applied to minimize heat losses, achieved using polyurethane. All the relevant data and technical specifications are sourced from a commercial data sheet, see Table 3.

Table 3. Piping system materials [34].

Material	Unit	Value	
Polypropylene	kg	1.13	Value estimated from technical sheet
Polyurethane	kg	1.45	Value estimated from technical sheet

A cylindrical-cavity receiver is used for its cost-effectiveness. The heat-transfer surface of this receiver consists of a coiled copper metal tube. A heat-transfer fluid flows within these coiled tubes to transfer the intense solar energy to the working fluid. The system presented here is designed to provide domestic hot water, with a temperature desired by the user of 45 °C. Thermia B oil, derived from highly refined mineral oils from crude oil, was chosen for this specific application. Considering the heat transfer tubes, a total of 20 litres of heat transfer fluid is required. To minimise heat loss from the cavity, it is assumed that the cavity receiver is insulated with mineral wool insulation material, with a 20-mm-thick layer of glass wool around the receiver, see Table 4.

Preprints (www.preprints.org) | NOT PEER-REVIEWED | Posted: 17 November 2023 doi:10.20944/preprints202311.1161.v1

Table 4. Solar receiver materials.

Material	Unit	Value	
Copper	kg	11.2	Value estimated from receiver geometry considering copper density equal to 8960 kg/m³[35]
AISI 310	kg	21.14	Value estimated from receiver geometry considering AISI 310 density equal to 7900 kg/m³[36]
Glass wool	kg	0.122	Value estimated from receiver geometry considering wool density equal to 20 kg/m³[37]
Thermal oil	kg	17.36	Value estimated considering thermal oil density equal to 868 kg/m³[38]

The geometrical parameters of the parabola used in the initial phase of this study mirror those of the parabola accessible at the Energy Center of the Politecnico di Torino. A thorough literature review was conducted, and some assumptions were made to complete the complete analysis of the system. Aluminium was chosen as the construction material for the solar dish (disc). The disc cover is 2 mm thick and is made of treated aluminium to increase reflection and concentration at the receiver. The support structure is made of stainless steel, see Table 5. There is a tracking mechanism and information about its construction support and the materials used is available directly from the manufacturer [39]: the material used is Fe360 structural steel.

Table 5. Parabolic dish materials.

Material	Unit	Value	Notes
Stainless steel	kg	592.5	Value calculated considering the available design of parabolic dish structure with stainless steel density equal to 8000 kg/m³[40]
Aluminium	kg	320	Value estimated through calculation of collector area and its thickness, considering aluminium density equal to 2710 kg/m³[41]
Glass	kg	20	Value estimated through calculation of collector area, with 2

			mm of glass thickness, considering glass density equal to 2500 kg/m³[42]
Structural steel	kg	0,9	Value calculated considering the available design of solar tracking system, considering structural steel density equal to 7850 kg/m³[43]

In OpenLCA software, the disposal of products at the end of their life cycle is facilitated using flows categorized as "waste." These waste flows need to be incorporated into the process's output. The method employed for end-of-life treatment is known as the Cut-off method. Under this approach, the model concludes with waste collection and treatment, excluding the recycling and the creation of new products [44]. End-of-life treatment was implemented for several materials, including copper, glass wool, stainless steel, the hot water tank, and aluminium. However, for certain materials, modelling end-of-life scenarios proved challenging due to the limited data available in the database and the absence of suitable proxies for their treatment. The final process, “System Use," pertains to the production of a single hot water tank. This analysis assumes that the entire system can operate efficiently for a duration of 30 years. The system's utilization for water production is anticipated to occur daily, with the capacity to produce one tank of hot water (190 litres) available for 255 out of 365 days in a year, equivalent to 69.86% of the year's days. In terms of system lifetime, this translates to 10,950 days or 7,650 operational days. Consequently, the production of one hot water tank contributes an equivalent of 1.30719E-4. The inputs to the use phase encompass all the processes previously described, including transportation, along with 190 litres of water. It is assumed that the entire system is manufactured 500 kilometres away from the usage location and is subsequently transported via road using articulated lorry transport. Notably, manual handling of the system is not considered due to a lack of available data on the subject. In summary, the use of the system encompasses the production of the solar collector, the production of the solar receiver, the production of the piping system, the production of the hot water tank storage, transportation from the manufacturing location to the usage site, the actual usage of the system, and the end-of-life disposal of components.

Model and LCA results

The choice of materials for the receiver was influenced by the maximum temperature derived from COMSOL Multiphysics simulations. This temperature is the result of the radiant flux striking the inner surfaces as well as the sides and bottom of the receiver after interception. When the radiant flux hits a given surface, a fraction of it is absorbed and the rest is reflected onto the other surfaces, including the aperture. If it is reflected off the receiver wall, the process is repeated. If it is reflected to the aperture, this fraction of radiant energy is lost to the environment - reflection losses. Reflection losses and reflection on the receiver surfaces depend on:

- The receiver shape and size
- The solar absorptance of the receiver inner surfaces
- The reflection type of the receiver inner surfaces, namely specular, specular with Gaussian scattering or Lambertian (Diffuse).

Therefore, the heat flux absorbed by the receiver is non-uniformly distributed across its inner surfaces, and this distribution is influenced by various factors. In this analysis, the focal plane is defined as the inner cylinder with a radius of 150 mm and a height of 230 mm. The figure below illustrates the resulting temperature distribution (Figure 5).

Preprints (www.preprints.org) | NOT PEER-REVIEWED | Posted: 17 November 2023 doi:10.20944/preprints202311.1161.v1

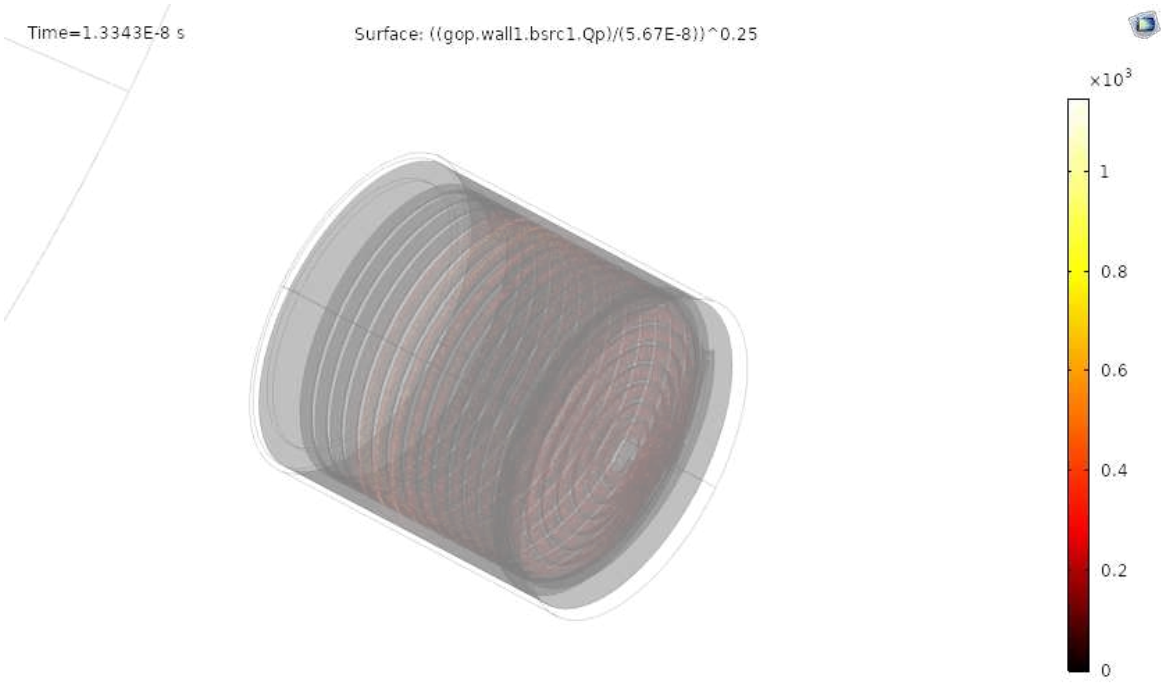

Figure 5. Temperature distribution inside cavity receiver.

The highest attained temperature within the cavity receiver registers at 873.75 °C (or 1146.9 K), accompanied by an average power of 7466.7 $\frac{kW}{m^2}$. To endure this temperature, an internal coil made of copper tubes, consisting of fourteen turns along the cavity's height, is employed. Copper is chosen due to its rapid heat transfer capabilities, owing to its excellent thermal conductivity. Additionally, its affordability is a noteworthy advantage, especially for the household sector. The maximum temperature reached inside the cavity receiver is 873.7 °C (or 1146.9 K), accompanied by an average power of 7466.7 kW/m^2. As can be seen from the figure, the maximum temperature is only reached at certain points. The distribution reached is therefore compatible with the type of material (copper tubes with fourteen wound coils) and the maintenance of the receiver structure is guaranteed. Copper was chosen for its rapid heat transfer capabilities and excellent thermal conductivity, see Table 6.

Table 6. Copper properties.

Physical propriety	Unit	Value
Density	kg/m^3	8960
Thermal conductivity	W/(mK)	386
Heat capacity at constant pressure	J/(kgK)	0.38

To improve the ability of the spirally wound copper tubes to effectively absorb solar radiation and reduce losses, it was decided to apply a black chrome coating to the copper surface $(Cr - Cr_2O_3)$. The black chrome coating has an emissivity of 0.09 and an absorbance of 0.84 [45]. The outer casing must be made of AISI 310 stainless steel, the main properties of which are given in Table 7. AISI 310 is an austenitic stainless steel with a high chromium and nickel content and a high carbon content. This type of steel offers excellent heat resistance, although it has a significantly lower thermal conductivity than copper.

Preprints (www.preprints.org) | NOT PEER-REVIEWED | Posted: 17 November 2023 doi:10.20944/preprints202311.1161.v1

Table 7. AISI 310 properties.

Physical propriety	Unit	Value
Density	kg/m³	7900
Thermal conductivity	W/(mK)	23.7
Heat capacity at constant pressure	J/(kgK)	610

As established above (Table 7), 7.71 kW are required to heat the water tank in one hour. In the context of the presented system, approximately 5 hours of radiation are required. This is based on an average heat source of 7.45 kW/m² inside the receiver, which has a surface area of 0.207 m². The system analysed for domestic hot water production operates without emissions during its use. However, emissions do occur during the production of these systems. The inventory collected for the life cycle assessment analysis includes all input and output components covering the entire life cycle of each modelled product. This inventory includes the flows of materials and energy exchanged between the system and the environment. Inputs are defined by the resources consumed, which include raw materials, energy, and land use, while outputs include emissions to air, water or soil. Due to the large list of inputs and outputs, a cutoff value of 1% was applied. The result was 297 input components and 1890 output components. Below is a summary of the top 10 components for reference.

Among the most used materials are hard coal, inert rock, water, natural gas and crude oil, see Table 8. These materials play a significant role in extraction and production processes. In contrast, other forms of renewable energy could be associated with the consumption of electricity during the manufacturing phase.

Table 8. Inputs obtained from inventory analysis and referred to the functional unit of the system.

	Input			
Flow	**Category**	**Sub - category**	**Unit**	Result
hard coal	Resources	From ground	MJ	3.9E+00
Inert rock	Resources	From ground	kg	3.9E+00
Water (rain water)	Resources	From water	kg	2.8E+00
Air	Resources	In air	kg	2.5E+00
Natural gas	Resources	From ground	MJ	2.1E+00
Crude oil	Resources	From ground	MJ	1.5E+00
Sea water	Resources	From water	kg	1.5E+00
Primary energy from hydro power	Resources	From water	MJ	7.5E-01
Primary energy from solar energy	Resources	From air	MJ	3.0E-01
Uranium	Resources	From ground	MJ	2.7E-01

The main pollutant is carbon dioxide, which can be attributed to energy production, see Table 9. Part of it comes from fossil fuels, while another part comes from the combustion or decomposition of organic materials. The analysis of the impact of each component starts with the raw materials, includes the manufacturing phase, transport from the factory to the assembly site and end-of-life treatment. In the use phase, water consumption was added, while maintenance was not included due to lack of data. The climate change impact category is represented with the EF Impact Assessment Model - Bern: Global Warming Potentials (GWP) over a 100-year time horizon and the indicator is expressed in terms of kg of CO_2 equivalent. End-of-life treatment was only applied to materials for which it was possible: copper, aluminium, steel, polyurethane, glass wool (Figures 6–9).

Preprints (www.preprints.org) | NOT PEER-REVIEWED | Posted: 17 November 2023 doi:10.20944/preprints202311.1161.v1

Table 9. Emissions to air and to water from main polluting elements obtained from inventory analysis and referred to the functional unit of the system.

	Emissions			
Flow	**Category**	**Sub - category**	**Unit**	Result
Carbon dioxide (fossil)	Emissions	Emissions to air	kg	6.51E-01
Carbon dioxide (biogenic)	Emissions	Emissions to air	kg	2.26E-02
Sulphur dioxide	Emissions	Emissions to air	kg	3.10E-03
Nitrogen dioxide	Emissions	Emissions to air	kg	1.45E-03
Carbon monoxide (fossil)	Emissions	Emissions to air	kg	1.26E-03
Nitrogen monoxide	Emissions	Emissions to air	kg	5.66E-05
Nitrous oxide	Emissions	Emissions to air	kg	1.09E-05
Nitrogen oxides	Emissions	Emissions to air	kg	9.24E-06
Carbon monoxide (biogenic)	Emissions	Emissions to air	kg	1.40E-06
Sulphate	Emissions	Emissions to air	kg	3.95E-07

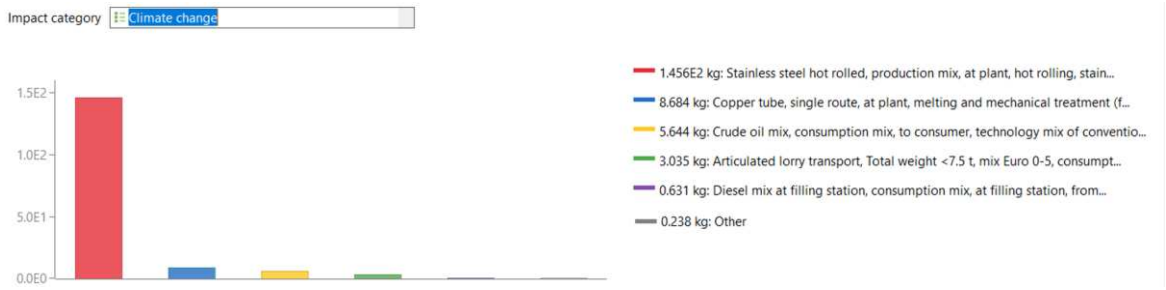

Figure 6. Climate change impact category for cavity receiver production.

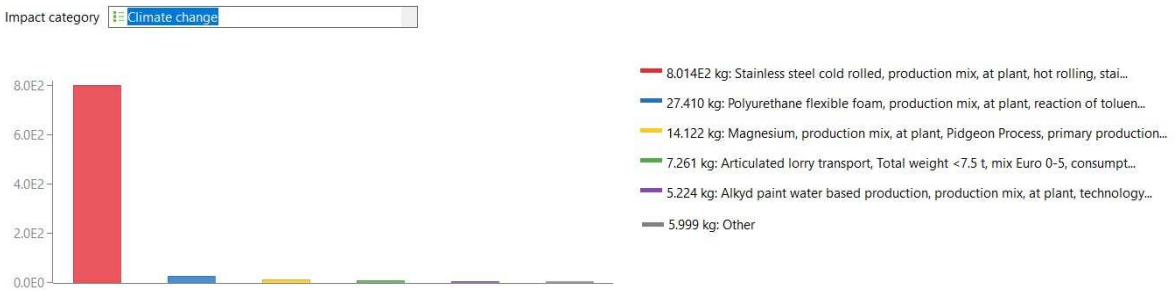

Figure 7. Climate change impact category for hot water tank production.

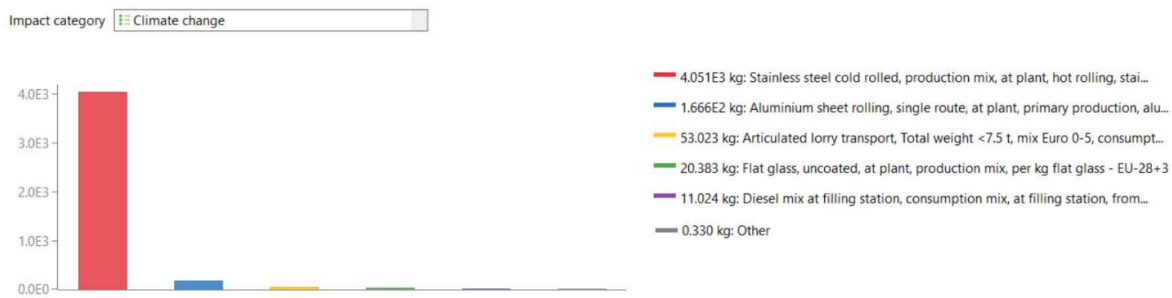

Figure 8. Climate change impact category for parabolic dish production.

Preprints (www.preprints.org) | NOT PEER-REVIEWED | Posted: 17 November 2023 doi:10.20944/preprints202311.1161.v1

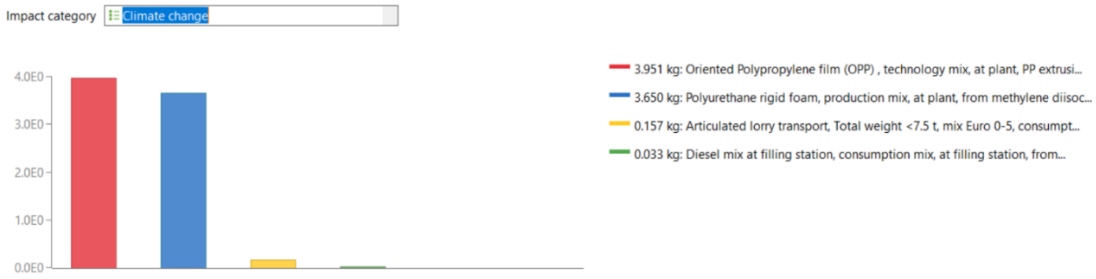

Figure 9. Climate change impact category for piping system production.

In every process, except for pipeline pipes, stainless steel production stands out as the most significant contributor to the climate change impact category. For both steel production technologies, hot-rolling and cold-rolling, the available dataset includes all relevant stages of the supply chain, with the process inventory being mainly based on industrial data. The data set for steel production is based on internationally recognised production processes linked to regional precursor chains. Although steel production is known for its energy intensity and significant greenhouse gas emissions, it is important to note that steel can be recycled. However, it should be noted that this analysis does not consider recycled steel as input material.

The process with the most significant impact in all categories, except for ozone depletion, is the manufacture of the dish, see Table 10. Steel stands out as the least environmentally friendly material due to its energy-intensive production. This observation extends to other impact categories, and since satellite dishes contain a substantial amount of steel, they also emerge as the main contributors to these impact categories. In contrast, for the ozone depletion indicator, the pipe manufacturing process takes the lead. This contribution can be attributed to the use of polyurethane as an insulating material. The available data set for this material covers the entire life cycle and the inventory comes from European industry data (EU-28+EFTA). The same amount of domestic hot water could be heated with a conventional natural gas boiler. Assuming a boiler efficiency of 93% and stoichiometric methane consumption, 1.6 kg of CO_2 will be emitted in one day. Assuming the same emissions for 30 years and considering the same number of days of operation of the solar dish, 12240 kg of CO_2 are emitted. This number results only from the operation phase of the system and is much larger than the number obtained from the production process of the four components of the solar dish analysed above.

Table 10. Comparison of the analysed components for the different impact categories.

Indicator	Parabolic dish	Hot water tank	Cavity receiver	Piping line	Unit
Acidification	32.303	6.413E+00	1.242E+00	0.017E+00	mol H+ eq
Climate change	4.30E+03	8.61E+02	1.64E+02	7.79E+00	kg CO_2 eq
Ecotoxicity, freshwater	2.61E+03	5.45E+02	1.05E+02	1.16E+00	CTUe
Eutrophication, freshwater	5.10E-03	1.56E-03	1.80E-04	3.62E-05	kg P eq
Human toxicity, cancer	4.90E-05	1.03E-05	2.08E-06	6.81E-08	CTUh
Human toxicity, non-cancer	1.90E-04	6.43E-05	1.35E-07	6.85E-07	CTUh
Ionising radiation, human health	7.54E+01	1.03E+01	3.02E+00	4.14E+02	kg U235 eq
Land use	5.82E+03	1.18E+03	1.97E+02	2.96E+01	
Ozone depletion	6.84E-08	3.17E-07	2.53E-09	6.67E-06	kg CFC-11 eq
Particulate matter	5.18E-04	1.04E-04	1.85E-05	1.51E-07	kg PM2.5 eq
Photochemical ozone formation	1.19E+01	2.33E+00	4.66E-01	1.40E-02	kg NMVOC eq

Preprints (www.preprints.org) | NOT PEER-REVIEWED | Posted: 17 November 2023 doi:10.20944/preprints202311.1161.v1

Resource use, fossil	4.91E+04	1.00E+04	2.58E+03	1.93E+02	MJ
Resource use, minerals, and metals	2.08E-01	4.10E-02	8.08E-06	3.52E-06	kg Sb eq
Water use	1.27E+03	2.59E+02	4.21E+01	1.42E+00	m^3

Conclusion

This study evaluates a thermal energy production system using a concentrating solar power system. The system runs on renewable solar energy, making its operational phase sustainable. However, its production phase involves non-renewable resources and emissions. The work is divided into two parts. In the first part, the geometry of the cavity receiver was analysed using COMSOL Multiphysics software to select suitable materials. A cylindrical cavity receiver was chosen, considering a balance between cost and efficiency. Copper was chosen for the heat transfer tubes due to its high thermal conductivity and cost-effectiveness. The outer casing of the cavity receiver is made of AISI 310 steel to withstand high temperatures but has a lower thermal conductivity than copper. It is insulated with 20 mm glass wool to minimise heat loss. The second part of the work involved the life cycle assessment (LCA) of the hot water production system using OpenLCA software. The LCA covered four main components: the solar dish, the solar receiver, the piping system, and the hot water tank. The materials for each component were selected based on commercial offers and scientific publications. For each component, the entire life cycle, including transport, was modelled. The LCA analysis explored various impact categories, highlighting stainless steel as the most polluting material among the selected components. Emissions could be reduced by using recycled materials. Despite emissions during the production phase, the solar dish represents a promising alternative to conventional hot water production systems. The study reveals that CO_2 emissions during the operational phase of conventional systems exceed those from the manufacture of the four analysed components combined. Technological advances have the potential to improve the cost-effectiveness and environmental compatibility of these systems. However, to comprehensively quantify the environmental impact of renewable energy systems, further research in the field of life cycle assessment (LCA) is needed.

Nomenclature

A	Area of the concentrator (m^2)
cp	waster specific heat (kJ/kg/K)
Co	Optical concentration ratio (-)
CSP	Concentrated Solar Power
CSR	Circumsolar ratio
D_c	Diameter of the dish (mm)
d_f	Diameter of the focal point (mm)
DHW	Domestic hot water
E	Thermal energy for the sensible storage
f	Focal distance (mm)
GHG	Greenhouse gases
l	Length of the receiver (mm)
LCA	Life Cycle Assessment
P	Power of the concentrator (kW)
q	Heat flux (W/m^2)
Q	Incoming solar power (kW)
SC	Solar Concentrator
SDH	Solar District Heating
TES	Thermal Energy Storage
Tmains	Aqueduct temperature (°C)
Tmax	Maximum temperature in the tank (°C)
Tmin	Minimum temperature (°C)

Tuse	Desired temperature in the tank (°C)
V	Tank volume for the sensible storage
φ_R	Rim angle (°)
y_R	Depth (mm)
ρ	Density (kg/m^3)

References

1. Delivering the European Green Deal, (2021). https://commission.europa.eu/strategy-and-policy/priorities-2019-2024/european-green-deal/delivering-european-green-deal_en (accessed November 14, 2023).
2. Five key areas for Europe's energy transition | McKinsey, (n.d.). https://www.mckinsey.com/capabilities/sustainability/our-insights/five-key-action-areas-to-put-europes-energy-transition-on-a-more-orderly-path (accessed November 14, 2023).
3. D. Gielen, F. Boshell, D. Saygin, M.D. Bazilian, N. Wagner, R. Gorini, The role of renewable energy in the global energy transformation, Energy Strategy Rev. 24 (2019) 38–50. https://doi.org/10.1016/j.esr.2019.01.006.
4. M. Hafner, S. Tagliapietra, The Global Energy Transition: A Review of the Existing Literature, in: M. Hafner, S. Tagliapietra (Eds.), Geopolit. Glob. Energy Transit., Springer International Publishing, Cham, 2020: pp. 1–24. https://doi.org/10.1007/978-3-030-39066-2_1.
5. IREES - Institut für Ressourceneffizienz und Energiestrategien GmbH, Comprehensive assessment of the potential for efficient heating and cooling for Germany, (n.d.). https://energy.ec.europa.eu/system/files/2022-05/DE%20CA%202020%20en.pdf (accessed November 14, 2023).
6. Heating, IEA. (n.d.). https://www.iea.org/energy-system/buildings/heating (accessed November 3, 2023).
7. Mapping and analyses of the current and future (2020 - 2030) heating/cooling fuel deployment (fossil/renewables), (n.d.). https://energy.ec.europa.eu/publications/mapping-and-analyses-current-and-future-2020-2030-heatingcooling-fuel-deployment-fossilrenewables-1_en (accessed November 3, 2023).
8. M. Temiz, I. Dincer, Development and assessment of an onshore wind and concentrated solar based power, heat, cooling and hydrogen energy system for remote communities, J. Clean. Prod. 374 (2022) 134067. https://doi.org/10.1016/j.jclepro.2022.134067.
9. G. Krajačić, M. Vujanović, N. Duić, Ş. Kılkış, M.A. Rosen, M. Ahmad Al-Nimr, Integrated approach for sustainable development of energy, water and environment systems, Energy Convers. Manag. 159 (2018) 398–412. https://doi.org/10.1016/j.enconman.2017.12.016.
10. K.E. N'tsoukpoe, S.C. Lekombo, F. Kemausuor, G.K. Ko, E.H.B. Diaw, Overview of solar thermal technology development and applications in West Africa: Focus on hot water and its applications, Sci. Afr. 21 (2023) e01752. https://doi.org/10.1016/j.sciaf.2023.e01752.
11. IEA SHC || Task 55 || Integration of Large SHC Systems into DHC Networks, (n.d.). https://task55.iea-shc.org/ (accessed November 3, 2023).
12. M. Abid, M.S. Khan, T.A. Hussain Ratlamwala, Thermodynamic Performance Evaluation of a Solar Parabolic Dish Assisted Multigeneration System, J. Sol. Energy Eng. 141 (2019). https://doi.org/10.1115/1.4044022.
13. K.S. Reddy, G. Veershetty, T. Srihari Vikram, Effect of wind speed and direction on convective heat losses from solar parabolic dish modified cavity receiver, Sol. Energy. 131 (2016) 183–198. https://doi.org/10.1016/j.solener.2016.02.039.
14. J. Coventry, C. Andraka, Dish systems for CSP, Sol. Energy. 152 (2017) 140–170. https://doi.org/10.1016/j.solener.2017.02.056.
15. A. Bianchini, A. Guzzini, M. Pellegrini, C. Saccani, Performance assessment of a solar parabolic dish for domestic use based on experimental measurements, Renew. Energy. 133 (2019) 382–392. https://doi.org/10.1016/j.renene.2018.10.046.
16. A. Marra, M. Santarelli, D. Papurello, Solar Dish Concentrator: A Case Study at the Energy Center Rooftop, Int. J. Energy Res. 2023 (2023) 1–18. https://doi.org/10.1155/2023/9658091.
17. D. Papurello, D. Bertino, M. Santarelli, CFD Performance Analysis of a Dish-Stirling System for Microgeneration, Processes. 9 (2021) 1142. https://doi.org/10.3390/pr9071142.
18. L. Borghero, Bressan, D. Ferrero, M. Santarelli, D. Papurello, Methane-Assisted Iron Oxides Chemical Looping in a Solar Concentrator: A Real Case Study, Catalysts. 12 (2022) 1477. https://doi.org/10.3390/catal12111477.
19. E. Montà, M. Santarelli, D. Papurello, Synthetic-Gas Production through Chemical Looping Process with Concentrating Solar Dish: Temperature-Distribution Evaluation, Processes. 10 (2022) 1698. https://doi.org/10.3390/pr10091698.
20. M. Perrero, D. Papurello, Solar Disc Concentrator: Material Selection for the Receiver, Energies. 16 (2023) 6870. https://doi.org/10.3390/en16196870.

21. How to Model Solar Concentrators with the Ray Optics Module, COMSOL. (n.d.). https://www.comsol.it/blogs/how-to-model-solar-concentrators-with-the-ray-optics-module/ (accessed June 20, 2022).
22. L.F. Cabeza, I. Martorell, L. Miró, A. Fernández, C. Barreneche, Introduction to thermal energy storage (TES) systems, in: Adv Therm Energy Storage Syst, 2015: pp. 1–28. https://doi.org/10.1533/9781782420965.1.
23. B. Corona, G. San Miguel, Life cycle sustainability analysis applied to an innovative configuration of concentrated solar power, Int. J. Life Cycle Assess. 24 (2019) 1444–1460. https://doi.org/10.1007/s11367-018-1568-z.
24. V. Piemonte, M.D. Falco, P. Tarquini, A. Giaconia, Life Cycle Assessment of a high temperature molten salt concentrated solar power plant, Sol. Energy. 85 (2011) 1101–1108. https://doi.org/10.1016/j.solener.2011.03.002.
25. N. Ko, M. Lorenz, R. Horn, H. Krieg, M. Baumann, Sustainability Assessment of Concentrated Solar Power (CSP) Tower Plants – Integrating LCA, LCC and LCWE in One Framework, Procedia CIRP. 69 (2018) 395–400. https://doi.org/10.1016/j.procir.2017.11.049.
26. Chr. Lamnatou, D. Chemisana, Concentrating solar systems: Life Cycle Assessment (LCA) and environmental issues, Renew. Sustain. Energy Rev. 78 (2017) 916–932. https://doi.org/10.1016/j.rser.2017.04.065.
27. E. Carnevale, L. Lombardi, L. Zanchi, Life Cycle Assessment of solar energy systems: Comparison of photovoltaic and water thermal heater at domestic scale, Energy. 77 (2014) 434–446. https://doi.org/10.1016/j.energy.2014.09.028.
28. Cathodic Protection - an overview | ScienceDirect Topics, (n.d.). https://www.sciencedirect.com/topics/physics-and-astronomy/cathodic-protection (accessed November 15, 2023).
29. S.S. Pathak, S.K. Mendon, M.D. Blanton, J.W. Rawlins, Magnesium-Based Sacrificial Anode Cathodic Protection Coatings (Mg-Rich Primers) for Aluminum Alloys, Metals. 2 (2012) 353–376. https://doi.org/10.3390/met2030353.
30. EMMETI-catalogo-tecnico-bollitori-e-serbatoi-ad-accumulo-2019.pdf, (n.d.). https://www.schede-tecniche.it/schede-tecniche-bollitori/EMMETI-catalogo-tecnico-bollitori-e-serbatoi-ad-accumulo-2019.pdf (accessed November 15, 2023).
31. Fiorini Industries, Rigid expanded polyurethane water storage tank data sheet - Fiorini Industries, (n.d.). https://www.fiorini-industries.com/en/download/root/eng/product_data_sheets_2018_rev1/without_prices/hot_water_storage_tanks.pdf (accessed November 15, 2023).
32. Interline-850-Potable-Water-Tanks.pdf, (n.d.). https://marinecoatings.brand.akzonobel.com/m/2daa08217affb122/original/Interline-850-Potable-Water-Tanks.pdf (accessed November 15, 2023).
33. Alkydprimer: Technical Data Sheet | PDF | Abrasive | Paint, Scribd. (n.d.). https://www.scribd.com/document/518722084/Download-2 (accessed November 15, 2023).
34. IDROTHERM-2000-Catalogo-Listino.pdf, (n.d.). https://agenzia-estesa.it/wp-content/uploads/2021/01/IDROTHERM-2000-Catalogo-Listino.pdf (accessed November 15, 2023).
35. Copper - Element information, properties and uses | Periodic Table, (n.d.). https://www.rsc.org/periodic-table/element/29/copper (accessed November 15, 2023).
36. Stainless Steel 310 - 1.4845 Data Sheet, Mater. UK. (n.d.). https://www.thyssenkrupp-materials.co.uk/stainless-steel-310-14845.html (accessed November 15, 2023).
37. ISOVER, SUIS_GB_Glass-wool_2016-03, (2016).
38. SHELL THERMIA, THERMIA-B.pdf, (n.d.). https://www.yairerez.co.il/wp-content/uploads/2019/10/THERMIA-B.pdf (accessed November 15, 2023).
39. ELMA srl, Electronic Machining - El.Ma Srl, Manuale uso e manutenzione - Concentratore solare a disco, Riva del Garda, 2019., 2019.
40. Density of Steel - The Physics Factbook, (n.d.). https://hypertextbook.com/facts/2004/KarenSutherland.shtml (accessed November 15, 2023).
41. The Density of Aluminium and its Alloys - thyssenkrupp Materials (UK), Mater. UK. (n.d.). https://www.thyssenkrupp-materials.co.uk/density-of-aluminium.html (accessed November 15, 2023).
42. Physical properties of glass | Saint Gobain Building Glass UK, (n.d.). https://www.saint-gobain-glass.co.uk/en-gb/architects/physical-properties (accessed November 15, 2023).
43. Fe Grade Steels, (n.d.). https://www.geocentrix.co.uk/help/content/items/steels/fe_grade_steels.htm (accessed November 15, 2023).
44. A. Nordelöf, S. Poulikidou, M. Chordia, F. Bitencourt de Oliveira, J. Tivander, R. Arvidsson, Methodological Approaches to End-Of-Life Modelling in Life Cycle Assessments of Lithium-Ion Batteries, Batteries. 5 (2019) 51. https://doi.org/10.3390/batteries5030051.

45. A. Hassan, C. Quanfang, S. Abbas, W. Lu, L. Youming, An experimental investigation on thermal and optical analysis of cylindrical and conical cavity copper tube receivers design for solar dish concentrator, Renew. Energy. 179 (2021) 1849–1864. https://doi.org/10.1016/j.renene.2021.07.145.